Available online at www.sciencedirect.com
SCIENCE DIRECT®
Pergamon
Acta Materialia 51 (2003) 4551–4561
Acta MATERIALIA
www.actamat-journals.com

Optimum glass formation at off-eutectic composition and its relation to skewed eutectic coupled zone in the La based La–Al–(Cu,Ni) pseudo ternary system

H. Tan [a], Y. Zhang [a], D. Ma [b], Y.P. Feng [c], Y. Li [a,*]

[a] *Department of Materials Science, National University of Singapore, Singapore 119260, Singapore*
[b] *Institute of Materials Research and Engineering, 3 Research Link, Singapore 117602, Singapore*
[c] *Department of Physics, National University of Singapore, Singapore 119260, Singapore*

Received 24 February 2003; received in revised form 25 March 2003; accepted 13 May 2003

Abstract

Glass formation and its relation to the dendritic and eutectic growth has been investigated for the $La_{100-x}[Al_{0.412}(Cu,Ni)_{0.588}]_x$ (x = 30–56.3) and $La_{86-y}Al_{14}(Cu,Ni)_y$ (y = 16–29) alloy systems. The experimental results show that in the La-rich pseudo ternary La–Al–(Cu,Ni) system, optimum glass formation actually occurs at an off-eutectic composition. A nearly fully amorphous rod with 12 mm in diameter can be obtained at an off-eutectic composition near $La_{62}Al_{15.7}(Cu,Ni)_{22.3}$, while only a 1.5 mm diameter rod can be obtained fully amorphous for the eutectic alloy $La_{66}Al_{14}(Cu,Ni)_{20}$. A strong dependence of GFA on the composition is observed for these alloys. In addition, formation of a composite (i.e. αLa dendrite reinforced glass matrix) in 12 mm diameter cast rods is observed over a wide range of composition, including the eutectic composition. It has been found that the GFA does not correlate well with the extent of the undercooled liquid region (ΔT_x) and is not even closely related to the reduced glass transition temperature (T_{rg}). These unusual observations in glass formation and its relation to the skewed eutectic coupled zone have been explained in terms of the competition between the growth of crystalline phases (i.e. eutectic and dendritic phases) and the formation of the amorphous phase.

Keywords: Bulk metallic glass; Composite; Solidification

1. Introduction

Glass forming ability (GFA) has been studied for several decades [1–12], and is currently of technical importance for the design and development of new bulk metallic glasses (BMGs). Several indicators have been proposed to predict glass forming ability [1,3,13–16], including reduced glass transition temperature T_{rg} (= T_g/T_l, T_g is glass transition temperature, and T_l is liquidus temperature) [13,14]. Turnbull's early work [13] on nucleation suggested that T_{rg} is a key indicator in determining GFA. Accordingly, the glass formation is always

* Corresponding author. Tel.: +65-6874-3348; fax: +65-6776-3604.
E-mail address: masliy@nus.edu.sg (Y. Li).

1359-6454/03/$30.00
doi:10.1016/S1359-6454(03)00291-X

associated with deep-eutectic and eutectic composition, since eutectic is always associated with the minimum liquidus temperature. However, Turnbull's work was based on the assumption that as long as nucleation of crystals (at a rate of $10^{-6}/cm^3$ s) is avoided, a glass will be formed, whereas once the nucleation rate is higher than $10^{-6}/cm^3$ s, the resulting alloy is assumed to be fully crystalline. Ulhmann [17] later considered both nucleation and growth of crystals and constructed a TTT diagram upon crystallization. Using this method, the critical cooling rate for glass formation was calculated to exhibit a qualitative correlation with the observed GFA [18]. Furthermore, Boettinger [19] pointed out that the limitation of crystal growth (dendrites and eutectic) should promote formation of metallic glasses. Accordingly, the competition between the formation of glass and the growth of crystals needs to be considered in the study of GFA.

In this paper, we report our experimental findings that the optimum composition for glass formation in the La based La–Al–(Cu,Ni) pseudo ternary eutectic system is actually at an off-eutectic composition. Under the consideration of the competition between the growth of crystals (dendrite and eutectic) and the formation of an amorphous phase, we relate the optimum glass formation at off-eutectic composition in this alloy system to the skewed eutectic coupled zone.

2. Experimental

La (99.9%), Al (99.9%), Ni (99.98%) and Cu (99.999%) were used as raw materials for arc melting (under a Ti-gettered argon atmosphere). Two series of alloys, $La_{100-x}[Al_{0.412}(Cu,Ni)_{0.588}]_x$ (x = 30–56.3) and $La_{86-y}Al_{14}(Cu,Ni)_y$ (y = 10–20) have been studied as shown in Fig. 1, in which Cu and Ni always have equal amounts. Ingots were cast by pouring the molten alloy into the cavity of a copper mold with diameters of 5–12 mm and 60 mm long. For comparison, glassy rods with diameters of 1, 1.5 and 2 mm, respectively, were prepared by chill casting. The corresponding glass transition temperature T_g and crystallization temperature T_x, onset melting temperature T_m (solidus) and offset melting temperature (liquidus) T_l were measured by differential scanning calorimetry (DSC) or differential thermal analysis (DTA) at a heating rate of 40 K/min. The resulting samples were sectioned transversely, mounted and polished for observation by scanning electron microscopy (SEM) and optical microscopy (OM). The degree of amorphicity of all samples was examined by X-ray diffractometry (XRD). Bridgman growth was carried out in alumina tubes with 3 mm internal diameter and a wall thickness of 0.5 mm. It involved remelting prior to steady withdrawal at constant pre-determined velocity in the range of 0.1–4.82 mm/s through a temperature gradient of 15 K/mm into a water bath. In addition, ribbon samples for these alloys were obtained by single roller melt-spinning in an argon atmosphere.

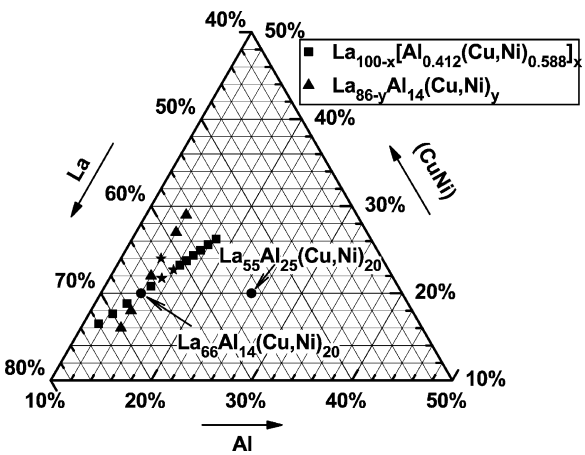

Fig. 1. Pseudo ternary La–Al–(Cu,Ni) diagram showing two series of alloy composition studied and the position of the eutectic alloy ($La_{66}Al_{14}(Cu,Ni)_{20}$). ∗ represents compositions with limiting size for glass formation larger than 10 mm. The reported glass forming alloy ($La_{55}Al_{25}(Cu,Ni)_{20}$) with 7 mm in diameter full amorphous structure is included for comparison.

3. Results

3.1. Results for $La_{100-x}[Al_{0.412}(Cu,Ni)_{0.588}]_x$ (x = 30–56.3) alloys

Fig. 2a shows T_l and T_m as a function of Al content indicating that the eutectic is at $La_{66}Al_{14}(Cu,Ni)_{20}$ (x = 34) with eutectic tempera-

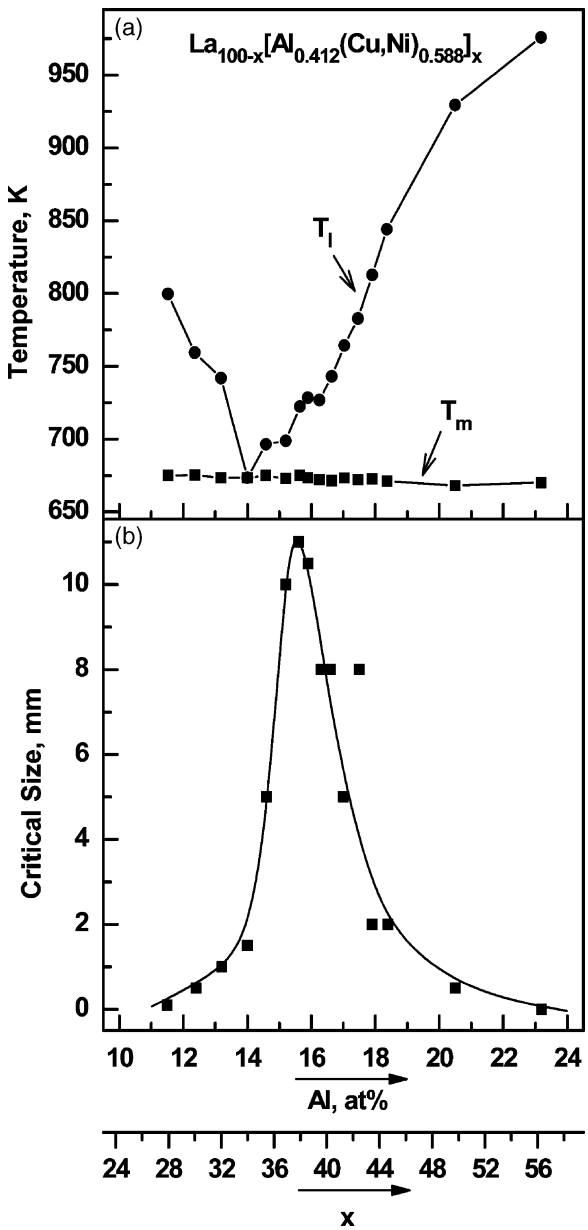

Fig. 2. (a) T_m and T_l and (b) limiting diameter for glass formation as a function of Al content in the $La_{100-x}[Al_{0.412}(Cu,Ni)_{0.588}]_x$ (x = 28–56.3) alloy series.

ture at around 675 K. Fig. 2b shows the critical diameter for full glass formation as a function of composition. It shows that the critical (limiting) size increased sharply from 1.5 mm at the eutectic composition $La_{66}Al_{14}(Cu,Ni)_{20}$ to 10–12 mm for an off-eutectic alloy around $La_{62}Al_{15.7}(Cu,Ni)_{22.3}$ (x = 38) and then decreased sharply again to 1.5 mm at $La_{56.3}Al_{18}(Cu,Ni)_{25.7}$ (x = 43.7). Fig. 3a–c shows SEM micrographs of cross-sections of the central parts of 12 mm diameter cast rods demonstrating a microstructure of a dendritic crystalline phase distributed in a uniform matrix for the $La_{66}Al_{14}(Cu,Ni)_{20}$ and $La_{70}Al_{12.4}(Cu,Ni)_{17.6}$ alloys, respectively (Fig. 3a and b), and a featureless microstructure for the $La_{62}Al_{15.7}(Cu,Ni)_{22.3}$ alloy (Fig. 3c). The XRD result shown in the inset of Fig. 3b indicates that the dendritic phase is hcp αLa and the corresponding DSC curve for the $La_{70}Al_{12.4}(Cu,Ni)_{17.6}$ and $La_{66}Al_{14}(Cu,Ni)_{20}$ as-cast samples confirms that the matrix is amorphous. The XRD result shown in the inset of Fig. 3c confirms that $La_{62}Al_{15.7}(Cu,Ni)_{22.3}$ is fully amorphous. Furthermore, the close resemblance between the DSC curves of the 12 mm rod and the melt-spun ribbon of the $La_{62}Al_{15.7}(Cu,Ni)_{22.3}$ alloy also confirms that the ingot is fully amorphous.

Fig. 4a depicts DSC curves for the fully amorphous state of the as-spun ribbons clearly showing that the crystallization behavior changed from multiple crystallization events to a major single event as the La content decreased. Fig. 4b shows that the values of T_{rg} and the extent of the supercooled liquid range ΔT_x (= $T_x - T_g$) exhibit maxima at about 14 and 17 at% Al, respectively, compared with the maximum in critical size for glass formation at around 15.5 at% Al. The above results are contrary to some early ones reported in the literature that bulk metallic glasses have a large ΔT_x with a single major crystallization event. Table 1 summarizes all the values of T_g, T_x, ΔT_x, T_m and T_l for the alloys studied.

3.2. Results for $La_{86-y}Al_{14}(Cu,Ni)_y$ (y = 16–29) alloys

Fig. 5a shows T_l and T_m as a function of (Cu,Ni) content. Fig. 5b shows DSC curves for the fully amorphous phase in these alloys clearly showing that the crystallization behaviour changed from multiple crystallization events to a major single event. Fig. 5c shows that T_{rg} has a maximum at the eutectic composition and the extent of the supercooled liquid region ΔT_x increased from 26

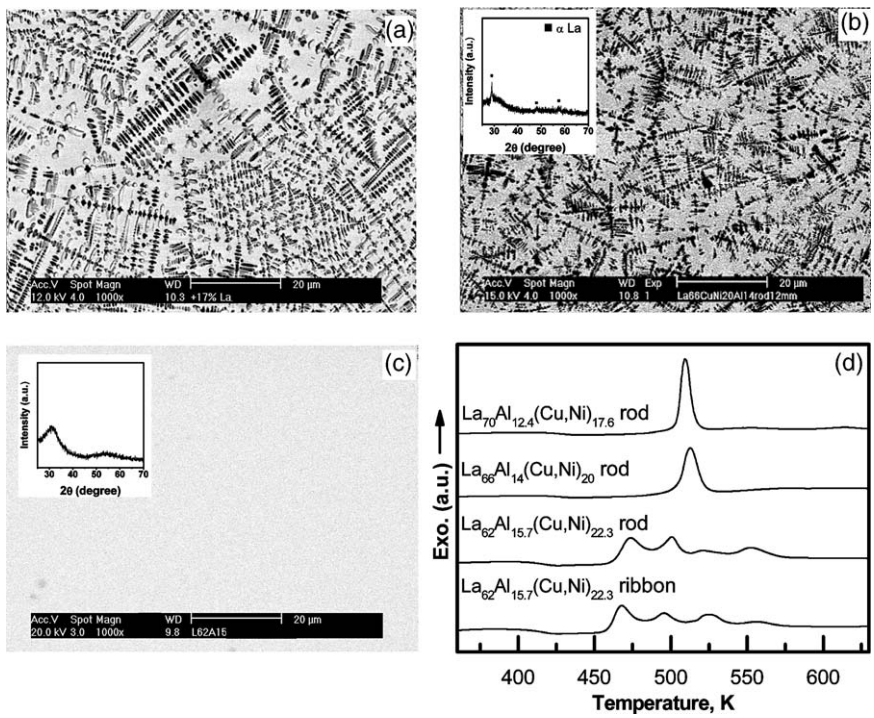

Fig. 3. SEM micrographs showing (a, b) composite of hcp αLa in amorphous matrix and (c) fully amorphous in the centre of 12 mm rods of $La_{70}Al_{12.4}(Cu,Ni)_{17.6}$, $La_{66}Al_{14}(Cu,Ni)_{20}$ and $La_{62}Al_{15.7}(Cu,Ni)_{22.3}$ alloys, respectively and (d) their corresponding DSC curves.

to 47 K when the (Cu,Ni) content increased from 16 to 29 at%. The values of T_m, T_l, T_g, T_x, T_{rg} and ΔT_x for these alloys are summarized in Table 1.

Casting of 12 mm diameter rods for these alloys was carried out to study their GFA. Fig. 6 shows typical SEM micrographs of the central parts of these ingots. Fig. 6a shows that $La_{70}Al_{14}(Cu,Ni)_{26}$ sample comprised dendrites in a featureless matrix. DSC curve for the $La_{70}Al_{14}(Cu,Ni)_{26}$ as-cast ingot (Fig. 6c) indicates that there is a substantial amount of amorphous phase in the matrix. The dendritic phase was identified by XRD as hcp αLa. Fig. 6b shows that $La_{62}Al_{14}(Cu,Ni)_{24}$ is nearly fully amorphous. This is confirmed by the XRD results (shown in the inset of Fig. 6b). The DSC results of the ingot and its melt-spun ribbon (Fig. 6c) also confirm this.

Our results clearly show that fully amorphous rod of 10–12 mm in diameter was obtained only at an off-eutectic composition, while in contrast a same sized composite rod (dendrites in an amorphous matrix) can be obtained for the eutectic $La_{66}Al_{14}(Cu,Ni)_{24}$ alloy. Furthermore, the optimum glass forming alloys have multiple crystallization peaks with a small undercooled liquid range (<40 K).

4. Discussion

4.1. Glass forming ability

The GFA of La based La–Al–Cu–Ni alloys has been studied extensively during the past decade [20–22]. The best manifestation of GFA for the quaternary La–Al–Cu–Ni alloys was a 7 mm diameter rod of $La_{55}Al_{25}Cu_{10}Ni_{10}$ alloy obtained by high pressure die-casting and this diameter was further improved to 9 mm in a quinary $La_{55}Al_{25}Cu_{10}Ni_5Co_5$ [21]. Our 10–12 mm diameter fully amorphous rods in quaternary La–Al–Cu–Ni are, to the best of our knowledge, the largest for La based alloy systems. It is also noticed that there is a strong dependence on the component elements, a

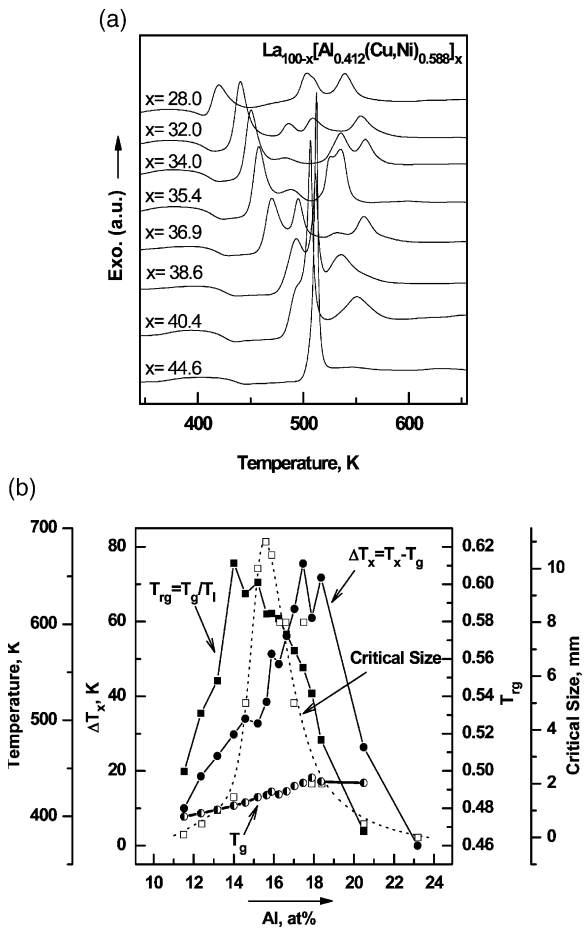

Fig. 4. (a) DSC curves of $La_{100-x}[Al_{0.412}(Cu,Ni)_{0.588}]_x$ (x = 28–56.3) alloys and (b)T_g, T_{rg} and ΔT_x as a function of Al content in the alloys.

narrow "U-shape" in terms of GFA (Fig. 2b). With only 2 at% changes in Al content (Fig. 2b), the limiting diameter for full glass formation for the $La_{100-x}[Al_{0.412}(Cu,Ni)_{0.588}]_x$ alloys change sharply from 1.5 to 10–12 mm. With a further increase in Al content, the limiting diameter dropped sharply to 1 or 2 mm (Fig. 2b). We have also noticed similar results for Pd based Pd–Cu–Ni–P alloys, where the critical cooling rate for glass formation increased sharply from ~2 K/s for the $Pd_{40}Cu_{30}Ni_{10}P_{20}$ alloy to 250 K/s for the $Pd_{42}Cu_{30}Ni_{10}P_{18}$ alloy with only a 2 at% difference in P content [23].

Figs. 4b and 5c show T_{rg} and ΔT_x (obtained from fully amorphous samples) as a function of composition, which clearly showed that the optimum glass forming alloy $La_{62}Al_{14}(Cu,Ni)_{24}$ has a ΔT_x of only 29 K, while the $La_{57}Al_{14}(Cu,Ni)_{29}$ alloy with maximal ΔT_x of 47 K exhibited a low GFA. Furthermore, our results indicate that the correlation between T_{rg} and GFA is also weak. As shown in Figs. 4b and 5c, the highest T_{rg} is found at the eutectic composition for these alloys, while the optimum GFA with low T_{rg} is at off-eutectic compositions.

4.2. Glass formation in alloy systems with a skewed eutectic coupled zone

There are two types of eutectic system in terms of their eutectic coupled zone which defines the composition and growth temperature (undercooling) range that leads to entirely eutectic growth. One is symmetrical about the eutectic composition, e.g. Al–Al_2Cu eutectic, and the other is skewed, e.g. Al–Si eutectic [24]. A symmetric coupled zone is associated with regular eutectic growth, which always includes the eutectic composition and reflects the similar growth behaviours of the two primary dendrite constituents [24]. Boettinger [19] showed in 1982 that the GFA and the corresponding composite formation in alloys with a symmetric eutectic coupled zone is around the eutectic. Our recent results for Pd based alloys [23] further confirmed his early analysis.

A skewed coupled zone (Fig. 7a), normally associated with irregular eutectic growth, is always skewed towards the faceted phase owing to its persistence of growth difficulty even at high undercoolings [24]. Whether the solidification microstructure is fully eutectic or dendrites plus eutectic depends on competitive growth between the primary phase and the eutectic [24]. This is governed by their growth temperatures as a function of growth rate (V) (Figs. 7c and d). For a given growth rate, the criterion for phase selection is established as the phase growing with the highest tip/front temperature will be the one observed. In this paper, we use cooling rate instead of growth rate since the temperature gradient in our Bridgman experiments is constant. For a system with a skewed coupled zone, growth temperature of the

Table 1
Results of DSC analysis at heating rate of 40 K/min and critical diameter for glass formation in La–Al–(Cu,Ni) alloys

Alloys	T_m, K	T_l, K	T_g, K	T_x, K	ΔT_x, K	T_{rg}	ΔH_x, J/g	GFA, mm
$La_{100-x}[Al_{0.412}(Cu,Ni)_{0.588}]_x$								
$La_{70.0}Al_{12.4}(Cu,Ni)_{17.6}$	675	759	403	422	19	0.53	50	0.5
$La_{68.0}Al_{13.2}(Cu,Ni)_{18.8}$	673	742	407	431	24	0.55	51	1
$La_{66.0}Al_{14.0}(Cu,Ni)_{20.0}$	674	674	405	431	29	0.60	52	1.5
$La_{64.6}Al_{14.6}(Cu,Ni)_{20.8}$	675	696	414	448	34	0.59	54	5
$La_{63.1}Al_{15.2}(Cu,Ni)_{21.7}$	673	699	420	459	39	0.60	48	10
$La_{62.0}Al_{15.7}(Cu,Ni)_{22.3}$	675	722	422	460	38	0.58	52	11
$La_{61.4}Al_{15.9}(Cu,Ni)_{22.7}$	674	729	426	477	51	0.58	53	10.5
$La_{60.5}Al_{16.3}(Cu,Ni)_{23.2}$	672	727	423	471	48	0.58	51	8
$La_{59.6}Al_{16.6}(Cu,Ni)_{23.8}$	672	743	426	482	56	0.57	52	8
$La_{58.6}Al_{17.0}(Cu,Ni)_{24.4}$	673	764	431	495	64	0.56	56	5
$La_{57.6}Al_{17.5}(Cu,Ni)_{24.9}$	672	783	435	510	75	0.56	58	8
$La_{56.5}Al_{17.9}(Cu,Ni)_{25.6}$	673	813	440	501	61	0.54	54	2
$La_{55.4}Al_{18.4}(Cu,Ni)_{26.2}$	671	844	436	508	72	0.52	45	2
$La_{50.2}Al_{20.5}(Cu,Ni)_{29.3}$	668	930	435	461	26	0.47	–	0.5
$La_{43.7}Al_{23.2}(Cu,Ni)_{33.1}$	670	976	–	–	–	–	–	0
$La_{86-y}Al_{14}(Cu,Ni)_y$								
$La_{70}Al_{14}(Cu,Ni)_{16}$	671	763	404	429	25	0.53	68	0.5
$La_{68}Al_{14}(Cu,Ni)_{18}$	671	724	405	431	26	0.56	61	1
$La_{66}Al_{14}(Cu,Ni)_{20}$	674	674	405	431	29	0.60	52	1.5
$La_{64}Al_{14}(Cu,Ni)_{22}$	676	715	411	439	28	0.57	74	8
$La_{62}Al_{14}(Cu,Ni)_{24}$	678	738	417	446	29	0.57	62	10
$La_{59}Al_{14}(Cu,Ni)_{27}$	678	773	422	457	35	0.55	64	5
$La_{57}Al_{14}(Cu,Ni)_{29}$	676	815	427	474	47	0.52	43	2

eutectic for the eutectic alloy is lower than that of the dendrite (α) when the cooling rate is higher ($\dot{T} > \dot{T}_1$) (Fig. 7c), leading to the coexistence of dendrites (α) and eutectic (Fig. 7a). Only at $\dot{T} < \dot{T}_1$, will a fully eutectic structure be obtained. As for the off-eutectic alloy as shown in Fig. 7b, its microstructure will be fully eutectic at sufficiently low cooling rate, dendrites (β) plus eutectic at intermediate rate, fully eutectic again at a higher cooling rate (Fig. 7a), and finally dendrites (α) plus eutectic at extremely high cooling rate. This microstructural change with increasing cooling rate is due to the relative growth temperatures as a function of cooling rate among the three competing constituents, i.e. α, β and eutectic (Fig. 7d) [24].

For an alloy system with a relatively high glass transition temperature (as shown in Fig. 7b), high cooling rate will lead to full glass or composite formation (Fig. 7b). In the case of skewed coupled zone, the eutectic in the eutectic alloy will be replaced by glass at cooling rates between $\dot{T}_c$ and $\dot{T}_a$ (Fig. 7c) as T_g is higher than the growth temperature of the eutectic, resulting in formation of a composite consisting of dendritic α plus glass. Here, $\dot{T}_c$ can be defined as the critical cooling rate for composite formation. Only when the cooling rate is higher than the critical rate for full glass formation, $\dot{T}_a$, will a fully amorphous structure form, as T_g is higher than the α dendrite growth temperature (and the eutectic growth temperature). As for an off-eutectic alloy, full glass formation will be achieved at $\dot{T} > \dot{T}'_a$ when T_g is higher than the growth temperature of the eutectics (and the α dendrites) (Fig. 7d). Here, the critical cooling rate for full glass formation $\dot{T}'_a$ is less than $\dot{T}_a$ in Fig. 7c, since the eutectic growth temperature and the glass transition temperature are less dependent on composition (in fact $\dot{T}'_a$ should be very close to $\dot{T}_c$ [19,24]). Consequently, the eutectic alloy always shows a poorer glass forming ability than the off-eutectic alloy, and the maximum GFA is at an off-eutectic composition as shown in Fig. 7b.

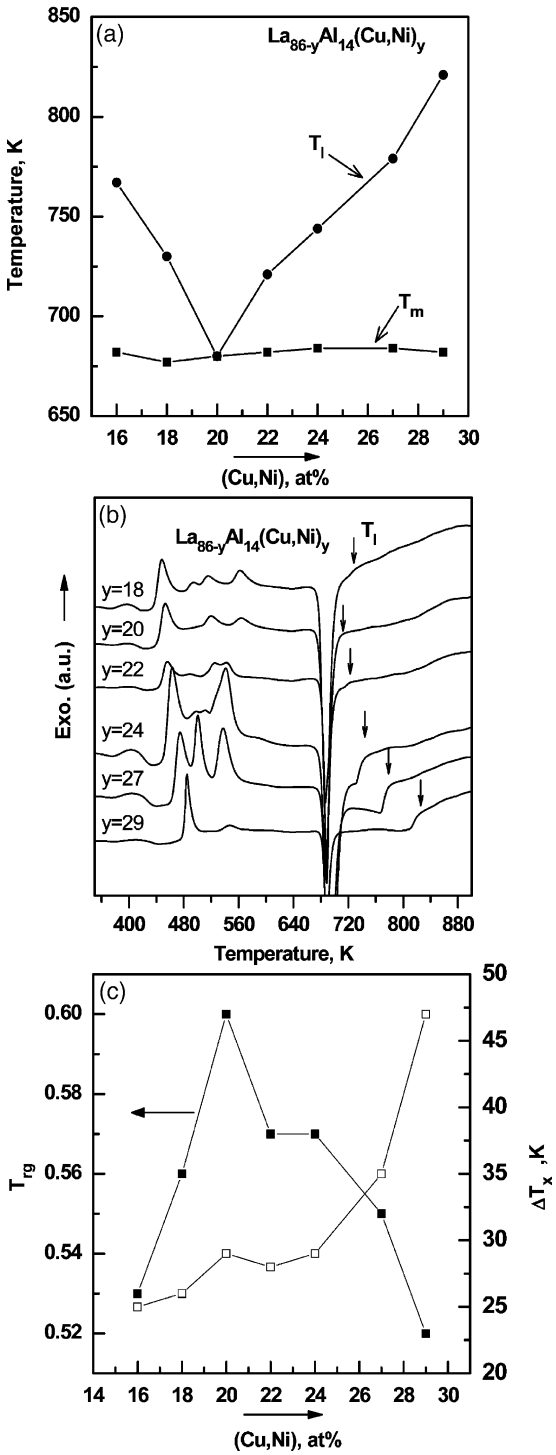

Fig. 5. (a) T_m and T_l, (c) T_{rg} and ΔT_x as a function of (Cu,Ni) content in the $La_{86-y}Al_{14}(Cu,Ni)_y$ (y = 16–29) alloys; (b) DSC curves of fully amorphous of $La_{86-y}Al_{14}(Cu,Ni)_y$ (y = 16–29) alloys.

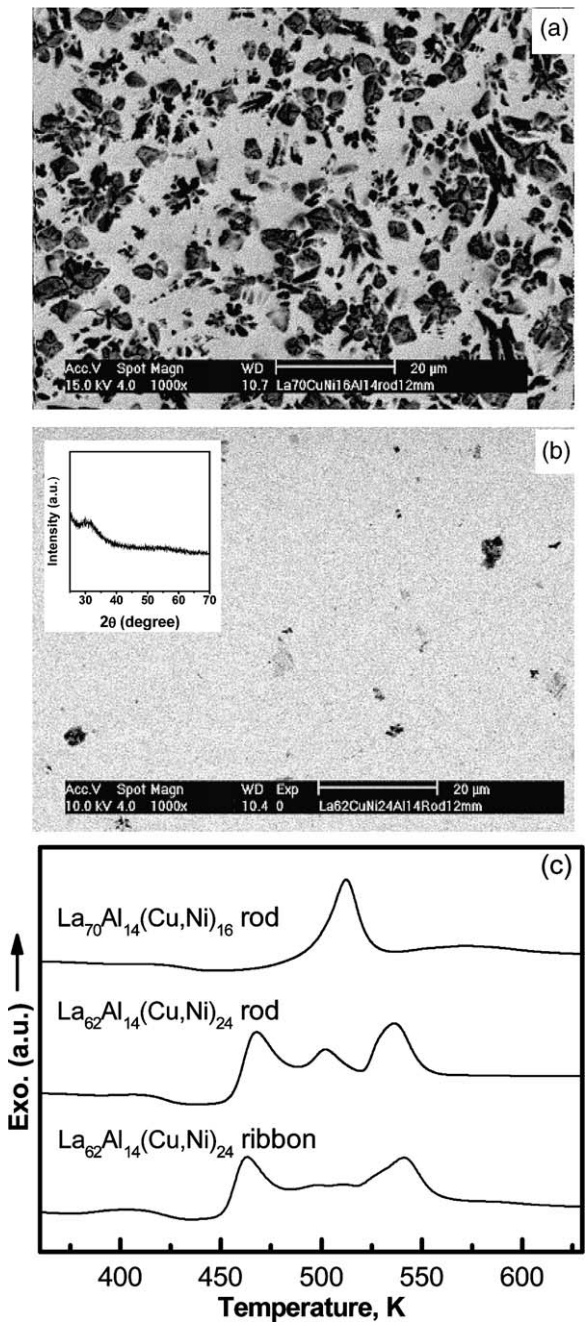

Fig. 6. SEM micrographs of central part of 12 mm rods for $La_{70}Al_{14}(Cu,Ni)_{16}$ showing hcp αLa in an amorphous matrix (a) and $La_{62}Al_{14}(Cu,Ni)_{24}$ showing almost fully amorphous (b), (c) and their corresponding DSC results.

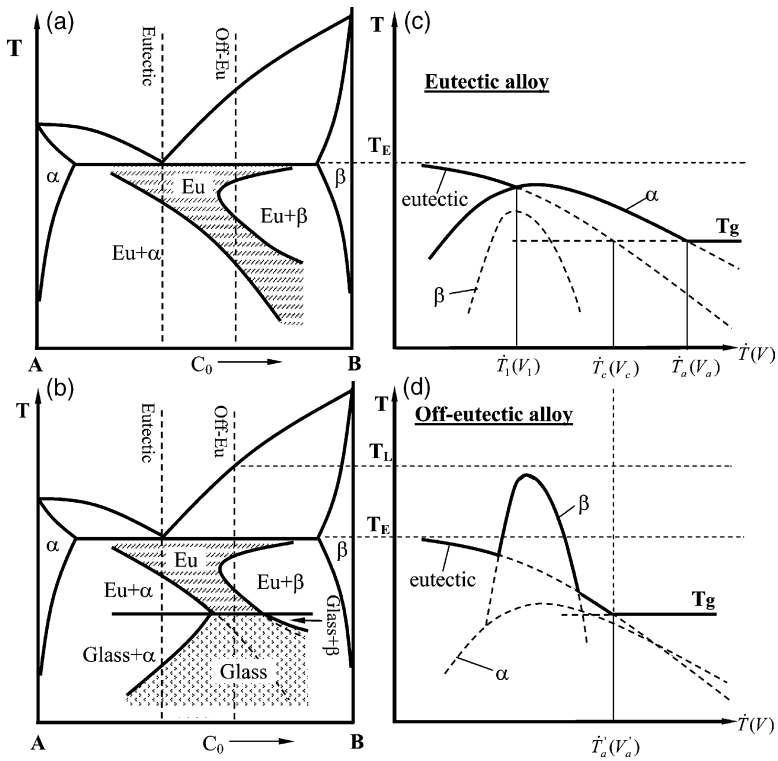

Fig. 7. Schematic diagrams showing skewed eutectic coupled zone and its relation to the glass forming ability: (a) a eutectic system with a skewed coupled zone; (b) glass forming and composite forming regions related to the skewed coupled zone; (c) growth temperature of the constituents as a function of cooling rate (growth rate) for the eutectic alloy and (d) growth temperature of the constituents as a function of cooling rate (growth rate) for an off-eutectic alloy.

4.3. Correlation for current system

In order to confirm the above analysis, corresponding microstructural evolution as a function of cooling rate in an alloy system with a skewed eutectic coupled zone (Figs. 7a and b) needs to be demonstrated, i.e.

(a) For the eutectic alloy, as the cooling rate increases, a sequential microstructural change should be as follows:

Fully eutectic→α dendrite plus eutectic→α dendrite plus amorphous→fully amorphous

(b) For the off-eutectic alloy with the best GFA, one can expect:

Fully eutectic→β dendrite plus eutectic→fully eutectic→fully amorphous.

Bridgman solidification with controlled growth rate/cooling rate was carried out for the $La_{86-y}Al_{14}(Cu,Ni)_y$ (y = 16–29) alloy series. The SEM micrograph (Fig. 8a) of the eutectic $La_{66}Al_{14}(Cu,Ni)_{20}$ alloy obtained at a cooling rate of 0.12 K/s exhibits a fully eutectic structure. As the cooling rate increased to 12 K/s, the resulting structure is primary αLa dendrites plus eutectic (Fig. 8b). With a further slight increase in cooling rate to 15 K/s, the structure turned dramatically to α dendrites plus amorphous phase, and only when it was increased to about 450 K/s, was a fully amorphous phase obtained [25]. DSC results in Fig. 8d confirmed that the samples solidified at 15 K/s and above contained a substantial amount of amorphous phase. This change in sequence of microstructure is entirely consistent with that illustrated in Fig. 7b for the eutectic alloy.

Fig. 9a shows an SEM micrograph of an off-eutectic $La_{62}Al_{14}(Cu,Ni)_{24}$ alloy solidified at 1.5

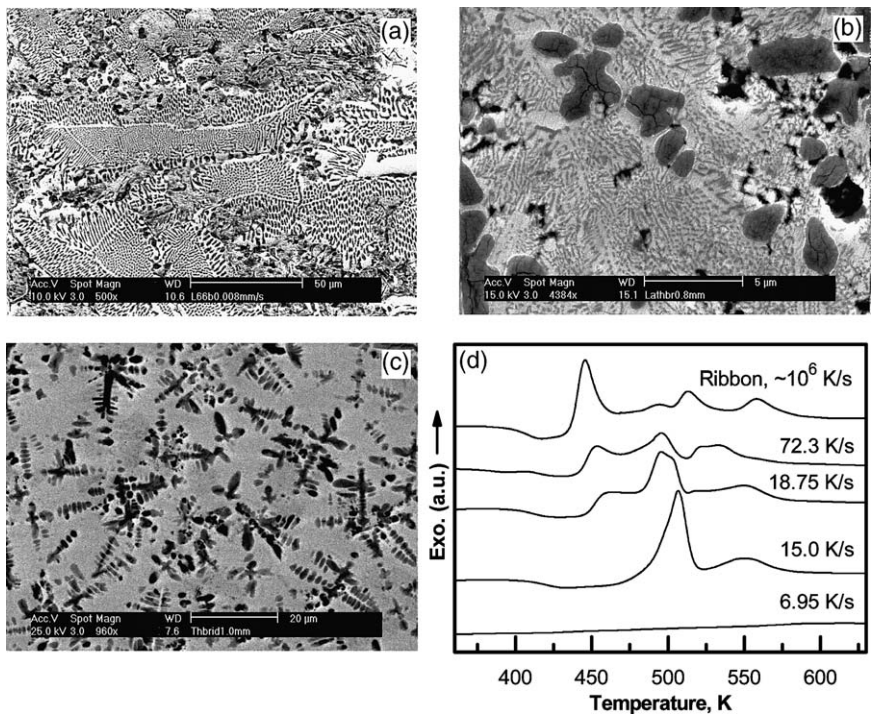

Fig. 8. SEM micrographs of the eutectic alloy $La_{66}Al_{14}(Cu,Ni)_{20}$ showing (a) fully eutectic morphology obtained at 0.015 K/s; (b) dendrites in a eutectic matrix at 12 K/s and (c) dendrites in an amorphous matrix at 15 K/s. DSC curves of this alloy at various cooling rates are shown in (d).

K/s showing faceted intermetallic primary phase and interdendritic eutectics. As the cooling rate is increased to 7.5 K/s, the microstructure developed as fully eutectics with very fine spacing (Fig. 9b). At 9 K/s, the microstructure became almost fully amorphous (Fig. 9c). Fig. 9d shows the DSC curves of these samples showing multiple crystallization peaks for the samples solidified at or higher than 9 K/s indicating the existence of a large amount of amorphous phase in these samples. But for the samples cooled at 7.5 K/s or lower only a flat line is obtained indicating no amorphous phase present in these samples. These DSC results are consistent with the observations shown in Figs. 9a–c. This structural evolution as a function of cooling rate again matches well with what has been illustrated in Fig. 7b for an off-eutectic alloy.

Our results suggest that the eutectic coupled zone associated with $La_{66}Al_{14}(Cu,Ni)_{20}$ eutectic point is skewed and that the optimum GFA is located at an off-eutectic composition. The above analysis clearly shows that the competition between growth of eutectics and dendrites and formation of amorphous phase is crucial in determining the GFA. Our earlier results for Pd based alloys [23] showed the same conclusion for an alloy system with a symmetric coupled zone, which is consistent with Boettinger's early analysis [19]. Both studies demonstrate that the GFA is strongly related to the eutectic coupled zone formation.

It has to be pointed out that one assumption for the current analysis is that T_g should be relatively high (Fig. 7), which implies that the value of T_{rg} should be high accordingly. This is consistent with the well-accepted fact that the higher the T_{rg} is, the better the GFA will be [13,14]. It can be anticipated that in searching for good glass formers, alloys with high T_{rg} should be found first (i.e. locating the eutectic composition). In the subsequent identification of the composition with the best GFA, the type of eutectic coupled zone needs to be considered, i.e. if the alloy system has a symmetric

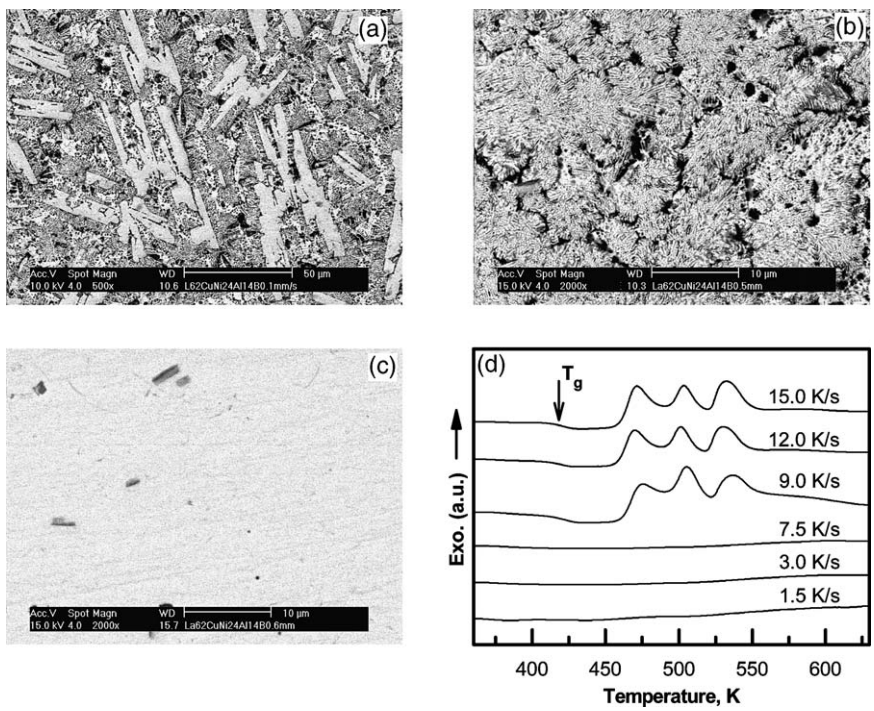

Fig. 9. SEM micrographs of the off-eutectic alloy $La_{62}Al_{14}(Cu,Ni)_{24}$ showing (a) intermetallic compound with interdendritic eutectics obtained at 1.5 K/s; (b) fully eutectic at 7.5 K/s and (c) fully amorphous structure at 9 K/s. Their corresponding DSC curves are shown in (d).

coupled zone, the optimum glass forming alloys should be around the eutectic composition [19]; and if the alloy system has a skewed coupled zone, the optimum glass forming alloys should be at an off-eutectic composition. It is inevitable that T_{rg} may not correlate well with GFA, particularly for systems exhibiting the skewed eutectic coupled zone (Figs. 4 and 5).

5. Conclusions

1. Our experimental results show that for the pseudo ternary La–Al–(Cu,Ni) system the optimum glass forming alloy is actually at an off-eutectic composition. A nearly fully amorphous rod of 10–12 mm in diameter can be obtained at an off-eutectic composition, while only a 1.5 mm diameter rod can be obtained fully amorphous for the $La_{66}Al_{14}(Cu,Ni)_{20}$ eutectic alloy. A strong dependence of GFA on the component element in these alloys, i.e. a narrow "U-shape", is observed. Formation of composite, i.e. dendrites in a glassy matrix, has been found over a large range of composition.
2. La–Al–(Cu,Ni) pseudo ternary alloys showed a skewed eutectic coupled zone. Our analysis suggests that for such a system, the optimum glass forming alloy should be at an off-eutectic composition.

Acknowledgements

We are grateful for fruitful discussions with Prof. H. Jones, Dr. W.J. Boettinger, Prof. W.L. Johnson and Dr. Z.P. Lu. We also appreciate very much helpful comments on the manuscript by Prof. H. Jones. YL and YZ would like to acknowledge financial support by Singapore-MIT Alliance (SMA).

References

[1] Inoue A. Acta Mater 2000;48:279.
[2] Johnson WL. MRS Bull 1999;24:42.
[3] Johnson WL. JOM-J Min Met Mat 2002;54:40.
[4] Kui HW, Greer AL, Turnbull D. Appl Phys Lett 1984;45:615.
[5] Peker A, Johnson WL. Appl Phys Lett 1993;63:2342.
[6] Liu CT, Chisholm MF, Miller MK. Intermetallics 2002;10:1105.
[7] Chen GL, Hui XD, He G, Bian Z. Mater Trans 2001;42:1095.
[8] He G, Echert J, Löser W, Schultz L. Nature Mater 2003;2:33.
[9] Wang WH, Wei Q, Bai HY. Appl Phys Lett 1997;71:58.
[10] Zhang Y, Pan MX, Zhao DQ, Wang RJ, Wang WH. Mater Trans JIM 2000;41:1410.
[11] Kang HG, Park ES, Kim WT, Kim DH, Cho HK. Mater Trans JIM 2000;41:846.
[12] Yi S, Park TG, Kim DH. J Mater Res 2000;15:2425.
[13] Turnbull D. Contemp Phys 1969;10:473.
[14] Lu ZP, Tan H, Li Y, Ng SC. Scripta Mater 2000;42:667.
[15] Lu ZP, Liu CT. Acta Mater 2002;50:3501.
[16] Chen W, Wang Y, Qiang J, Dong C. Acta Mater 2003;51:1899.
[17] Ulhmann DR. J Non Cryst Solids 1972;7:337.
[18] Davies HA. Rapidly quenched metals III, p. 1. London: The Metals Society, 1978.
[19] Boettinger WJ. In: Kear KH, Giessen BC, Cohen M, editors. Rapidly solidified amorphous and crystalline alloys. Elsevier Science Publishing; 1982. p. 15.
[20] Inoue A, Zhang T, Masumoto T. Mater Trans JIM 1990;31:425.
[21] Inoue A, Nakamura T, Sugita T, Zhang T, Masumoto T. Mater Trans JIM 1993;34:351.
[22] Lu ZP, Goh TT, Li Y, Ng SC. Acta Mater 1999;47:2215.
[23] Hu X, Ng SC, Feng YP, Li Y. Acta Mater 2003;51:561.
[24] Kurz W, Fisher DJ. Fundamentals of solidification, 4th ed. Switzerland: Trans Tech, 1998.
[25] Tan H, Zhang Y, Feng YP, Li Y. Intermetallics 2002;10:1203.